British Geological Survey
NATURAL ENVIRONMENT RESEARCH COUNCIL

The Moidart earthquakes of 4 August 2017

Earth Hazards Programme

Open Report OR/17/062

BRITISH GEOLOGICAL SURVEY

EARTH Hazards PROGRAMME

OPEN REPORT OR/17/062

The Moidart earthquakes of 4 August 2017

B Baptie, G Ford, D Galloway

The National Grid and other Ordnance Survey data © Crown Copyright and database rights 2017. Ordnance Survey Licence No. 100021290 EUL.

Keywords

Earthquakes; faults; seismotectonics .

Bibliographical reference

BAPTIE, B, FORD, G, Galloway, D. 2017. The Moidart Earthquakes of 4 August 2017. *British Geological Survey Open Report*, OR/17/062. 25pp.

Copyright in materials derived from the British Geological Survey's work is owned by the Natural Environment Research Council (NERC) and/or the authority that commissioned the work. You may not copy or adapt this publication without first obtaining permission. Contact the BGS Intellectual Property Rights Section, British Geological Survey, Keyworth, e-mail ipr@bgs.ac.uk. You may quote extracts of a reasonable length without prior permission, provided a full acknowledgement is given of the source of the extract.

Maps and diagrams in this book use topography based on Ordnance Survey mapping.

© NERC 2017. All rights reserved

Keyworth, Nottingham British Geological Survey 2017

BRITISH GEOLOGICAL SURVEY

The full range of our publications is available from BGS shops at Nottingham, Edinburgh, London and Cardiff (Welsh publications only) see contact details below or shop online at www.geologyshop.com

The London Information Office also maintains a reference collection of BGS publications, including maps, for consultation.

We publish an annual catalogue of our maps and other publications; this catalogue is available online or from any of the BGS shops.

The British Geological Survey carries out the geological survey of Great Britain and Northern Ireland (the latter as an agency service for the government of Northern Ireland), and of the surrounding continental shelf, as well as basic research projects. It also undertakes programmes of technical aid in geology in developing countries.

The British Geological Survey is a component body of the Natural Environment Research Council.

British Geological Survey offices

BGS Central Enquiries Desk

Tel 0115 936 3143 Fax 0115 936 3276

email enquiries@bgs.ac.uk

Environmental Science Centre, Keyworth, Nottingham NG12 5GG

Tel 0115 936 3241 Fax 0115 936 3488

email sales@bgs.ac.uk

The Lyell Centre, Research Avenue South, Edinburgh EH14 4AP

Tel 0131 667 1000 Fax 0131 668 2683

email scotsales@bgs.ac.uk

Natural History Museum, Cromwell Road, London SW7 5BD

Tel 020 7589 4090 Fax 020 7584 8270

Tel 020 7942 5344/45 email bgslondon@bgs.ac.uk

Columbus House, Greenmeadow Springs, Tongwynlais, Cardiff CF15 7NE

Tel 029 2052 1962 Fax 029 2052 1963

Maclean Building, Crowmarsh Gifford, Wallingford OX10 8BB

Tel 01491 838800 Fax 01491 692345

Geological Survey of Northern Ireland, Department of Enterprise, Trade & Investment, Dundonald House, Upper Newtownards Road, Ballymiscaw, Belfast, BT4 3SB

Tel 028 9038 8462 Fax 028 9038 8461

www.bgs.ac.uk/gsni/

Parent Body

Natural Environment Research Council, Polaris House, North Star Avenue, Swindon SN2 1EU

Tel 01793 411500 Fax 01793 411501

www.nerc.ac.uk

Website www.bgs.ac.uk

Shop online at www.geologyshop.com

Contents

FIGURES

Summary

The Moidart earthquake of 4 August 2017 (4.0 ML) was the largest earthquake in Scotland for 18 years. The earthquake was felt widely across the west of Scotland. Only five other earthquakes of this size or greater have been observed in the period of instrumental recording from 1970 to present. Historical observations and instrumental recordings have been used to estimate that an earthquake of 4.0 ML or greater occurs somewhere in Scotland roughly every 8-9 years on average.

The earthquake hypocentre was calculated using an iterative linearized method. The results suggest that the earthquake occurred in the mid-Crust at a depth of approximately 12 km. This is largely consistent with observed focal depths for other earthquakes in the region, which are distributed throughout the upper 20 km of the Crust.

The strong similarity between the recorded ground motions from the mainshock and the four recorded aftershocks suggests that they all occurred within a small source volume, of the order of a few hundred metres in extent and had similar source mechanisms.

The modelled source displacement spectra provide a good fit for the observed displacement spectra and suggest a moment magnitude (Mw) of 3.6 ± 0.1. This is slightly less than that expected for an earthquake with a local magnitude of 4.0 ML using commonly used empirical relationships relating local and moment magnitude, which gives an expected moment magnitude of 3.7.

The calculated focal mechanism suggests that the earthquake resulted from strike-slip faulting on a fault plane that strikes either SW-NE or NW-SE and dips steeply, although the dip of both fault planes is rather poorly constrained. This is in good agreement with focal mechanisms calculated for other earthquakes across the region, which all show similar solutions.

Seismicity in northwest Scotland is clustered around a number of large, steeply dipping major faults that strike either NE-SW or NW-SE suggesting that earthquake activity across the region is driven by reactivation of such fault systems by deformation associated with first-order plate motions rather than deformation associated with glacioisostatic recovery.

Although there are no mapped major fault systems in the immediate vicinity of the Moidart earthquake, it seems likely that the earthquake also occurred on a steeply dipping fault that strikes either NE-SW or NW-SE but remains unmapped.

1 Introduction

On 4 August 2017 at 14:43 UTC, an earthquake of magnitude 4.0 ML occurred in the locality of Moidart on the west coast of mainland Scotland (Figure 1). The epicentre was approximately 22 km south of Mallaig, 50 km west of Fort William and 145 km northwest of Glasgow. The earthquake was the largest event in the region since a magnitude 4.1 earthquake near Oban on 29 September 1986 and it was the felt widely across the west of Scotland.

The earthquake was followed by at least four aftershocks, the largest of which had a magnitude of 3.4 ML and which occurred two minutes after the mainshock. The two largest aftershocks were also felt by people across the region.

Analysis of the BGS earthquake catalogue shows that there have been only five other earthquakes with magnitudes of 4 ML or above in the period of instrumental monitoring from 1970 to present. The largest of these was a magnitude 4.4 ML earthquake near Kintail in 1974. This was one of a sequence of over 20 earthquakes that occurred over several months in 1974/1975. Two other earthquakes in this sequence also had magnitudes of above 4.0 ML. A magnitude 4.1 ML earthquake near Oban in 1986 was 24 km south-southeast of the Moidart earthquake. More recently, a magnitude 4.0 ML earthquake occurred near Arran in 1999. As a result, the Moidart earthquake of 4 August 2017 was the largest earthquake in Scotland in 18 years and, as such is a relatively rare event.

Similarly, historical observations of earthquake activity in Scotland date back to the 16th century (Musson, 1996). These show that despite many accounts of earthquakes felt by people, damaging earthquakes are relatively rare. Scotland's largest recorded earthquake, a magnitude 5.2 ML event in Argyll in 1880, was 75 km to the southeast of the Moidart earthquake. Only two other earthquakes with a magnitude of 5.0 ML or greater have been observed in the last 400 years. As a result, the risk of damaging earthquakes is low.

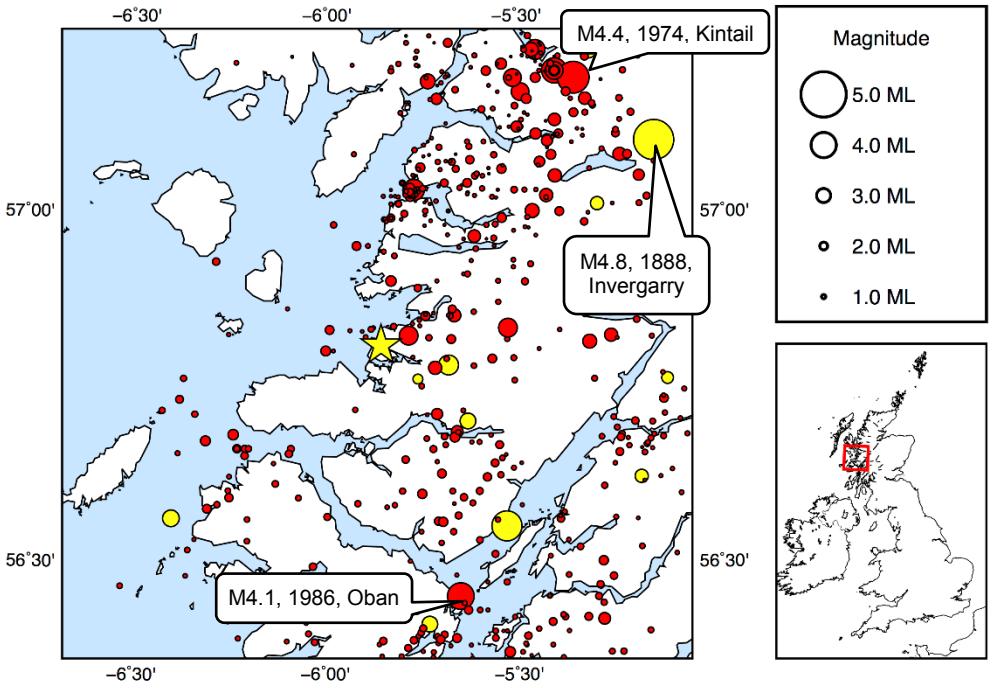

Figure 1. Instrumentally recorded earthquakes (red circles), from 1970 to present, and historical earthquakes (yellow circles), from 1700 to 1969, within a 100 km square centred on the epicentre of the Moidart earthquake of 4 August 2017 (yellow star). Circles are scaled by magnitude.

Musson (1994) lists 19 earthquakes with magnitudes of 4.0 ML or above in the period from 1800 to 1969. Combining these with the six instrumentally recorded earthquakes ≥4.0 ML suggests that there is an earthquake of this magnitude or greater somewhere in Scotland roughly every 8-9 years.

The aim of this report is to provide an overview of the source parameters determined for the Moidart earthquake along with an interpretation of the available macroseismic data.

2 Earthquake Location

Ground motions from the earthquake were recorded across the UK by seismometers operated by BGS at distances of more than 700 km. Figure 2 shows these ground motions as a function of time and distance from the epicentre. P-wave and S-wave arrivals are well-recorded. The first aftershock is clearly visible approximately two minutes after the mainshock.

P-wave phase arrival times were measured at 27 recording stations and S-wave arrivals measured at 6 recording stations giving 33 phases to determine the earthquake hypocentre. In addition,

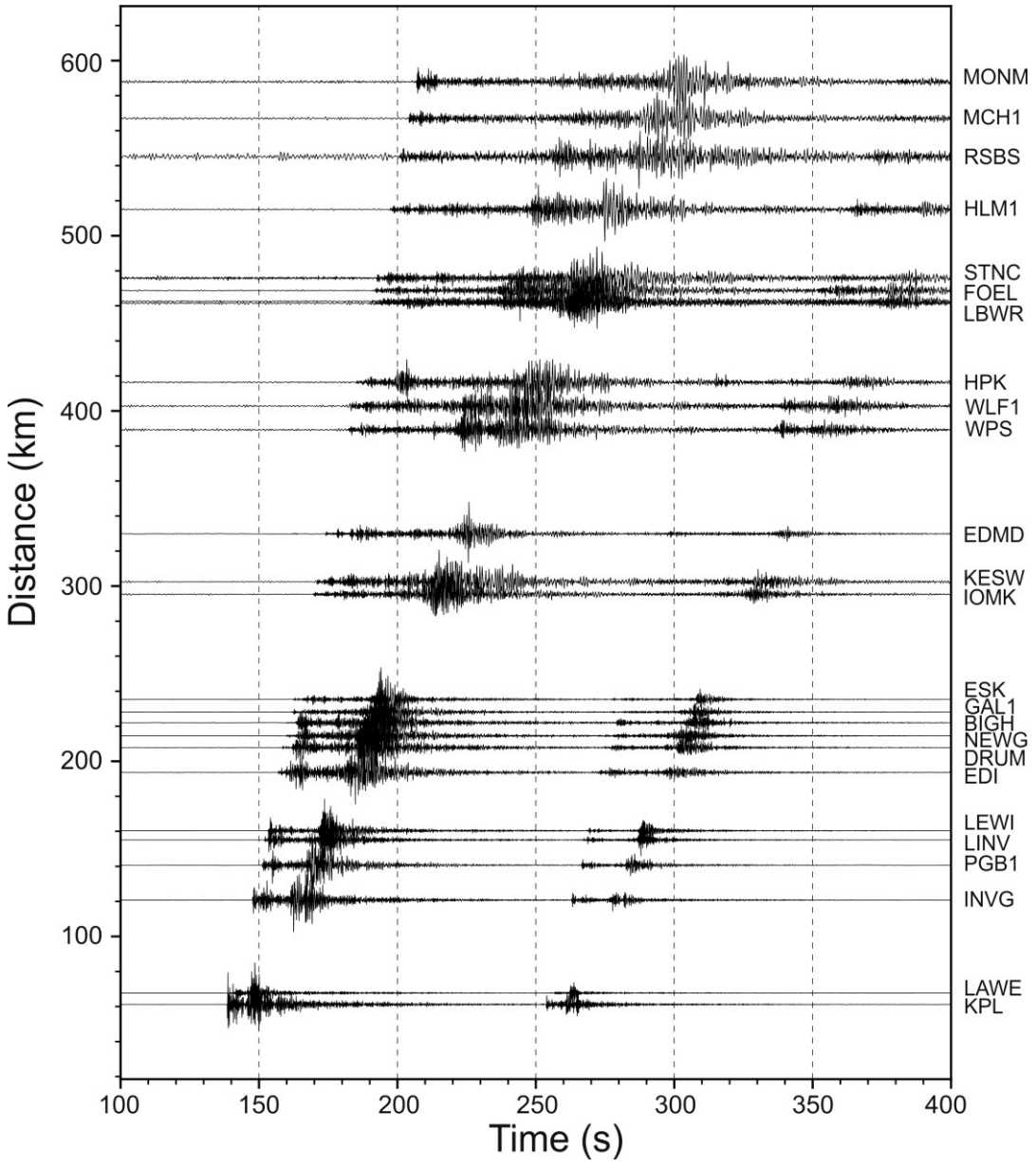

Figure 2. Ground motions for the Moidart earthquake of 4 August 2017. Recordings are shown as a function of increasing distance.

amplitudes to determine magnitude were measured on the horizontal components at 24 stations. The stations used for each are shown in Figure 3.

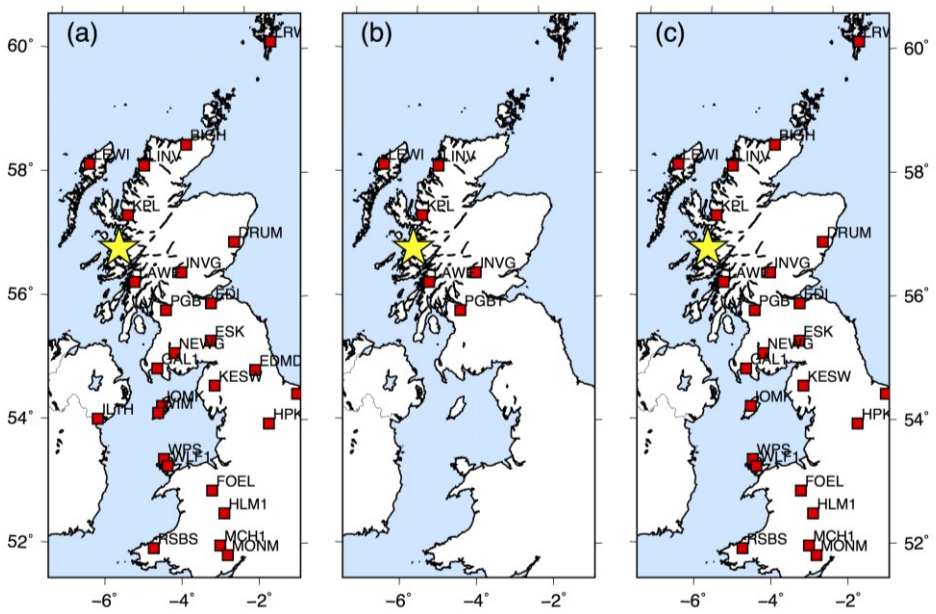

Figure 3. Stations with phase arrivals used to determine the location and magnitude for the earthquake. (a) Stations with P-wave arrivals. (b) Stations with S-wave arrivals. (c) Stations with a measured amplitude.

The closest seismometer to the epicentre is KPL at Plockton, 61 km to the north. The most distant station used was Monmouth almost 600 km to the south.

Table 1. Crustal velocity model used in earthquake location (Bamford et al., 1978; Assumpcão and Bamford, 1978)

Depth to top of layer (km)	P-wave velocity (km/s)	Vp/Vs
0.00	4.00	1.73
2.52	5.90	1.73
7.55	6.45	1.73
18.87	7.00	1.73
34.15	8.00	1.73

The arrival time data were input to the HYPOCENTER location algorithm (Lienert et al., 1986) to determine the earthquake hypocentre. In the absence of any definitive crustal velocity model for this area, from refraction or other sources, we used the 1-D velocity model shown in Table 1, determined from the LISPB refraction experiment (Bamford et al., 1978; Assumpcão and Bamford, 1978), over northern Britain. Strictly speaking, this model is valid only for the Midland Valley region of Scotland and contains a near-surface low velocity zone; however, the model has been widely used to locate earthquakes throughout Scotland, so this is model used for consistency. and has given reasonable results. An additional weighting factor based on the distance parameters *XNEAR* and *XFAR*, where the weight is linearly decreased from 1 to 0 between *XNEAR* and *XFAR*, was used to systematically reduce weighting with distance and is typically applied to reduce the effect of lateral heterogeneity in the velocity model. In this case, an *XNEAR* of value 300 km and an *XFAR* value of 600 km were applied.

Date	Time	Latitude	Longitude	Depth	ML	Npha	GAP	RMS	ERX	ERY	ERZ
04/08/2017	14:43:38.71	56.805	-5.888	12.2	4.0	33	153	0.41	7.0	1.7	4.9

Table 2. Earthquake hypocentre determined using the HYPOCENTER location algorithm.

Details of the best-fitting hypocentre are given in Table 2, together with the azimuthal gap, the root-mean-square (RMS) travel time residual and the horizontal and vertical errors in the hypocentre. The azimuthal gap is the largest azimuthal gap between azimuthally adjacent stations, and a value of 153° is relatively large and may lead to higher than desirable location errors. The RMS residual, measured in in seconds, provides a measure of the fit of the observed arrival times to the predicted arrival times for the given location and chosen velocity model. The horizontal and depth errors are determined from projections of the 95% confidence ellipsoid, assuming that the measurement errors are normally distributed. The size of the confidence regions depends on the variance and is computed using the $\chi 2$ statistic (Evernden, 1969). The orientation of the error ellipsoid depends on both the number and geometry of the recording stations. The hypocentre and the 95% confidence ellipsoid are shown in Figure 4.

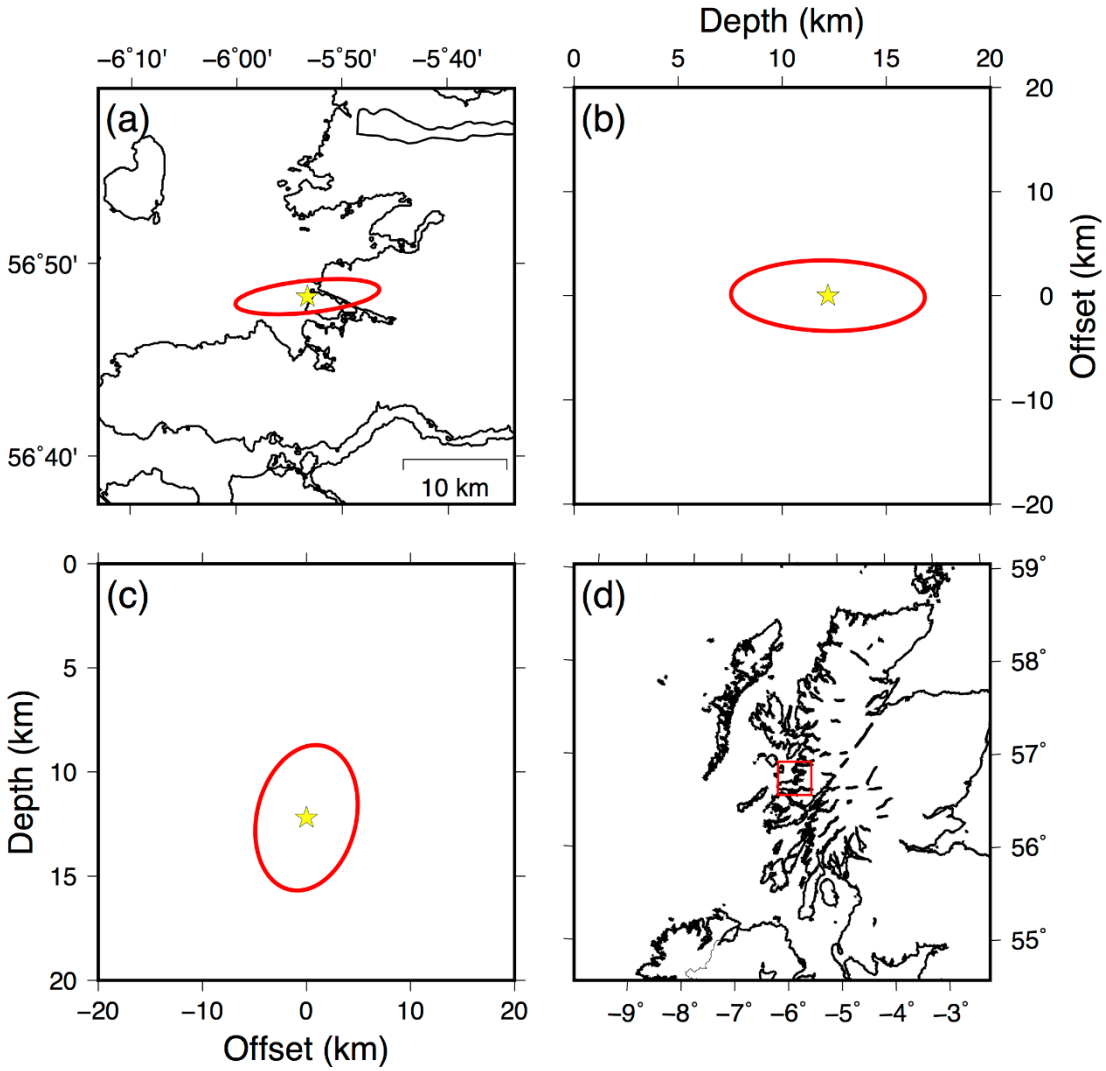

Figure 4. Projections of 95% confidence ellipsoid for the calculated hypocentre in: (a) the horizontal (XY) plane; (b) the YZ plane; and (c) the XZ plane. Each plane shows an area of 20 km by 20 km. (d) Shows the location of (a).

The horizontal errors in X (EW) and Y (NS) are ±7.0 km and ±1.7 km. The error is much larger in the EW direction primarily as a result of the distribution of stations and the large azimuthal gap.

It is important to note that the modelling errors of calculated travel times depend strongly on the choice of velocity model.

The source depth was determined at 12.2 km with a corresponding error of ±4.9 km. However, the nearest station to the epicentre is 61 km to the north, where both P- and S-wave arrivals were recorded. Considering the uncertainties associated with the 1-D velocity model, we conclude that the earthquake depth is likely to be poorly constrained. To further examine the depth resolution, we determined RMS error as a function of depth in the 0 to 30 km range with a spacing of 1 km. The results are shown in Figure 5 and display a well-defined minimum at 12 km, supporting the conclusion that the earthquake occurred in the mid-crust.

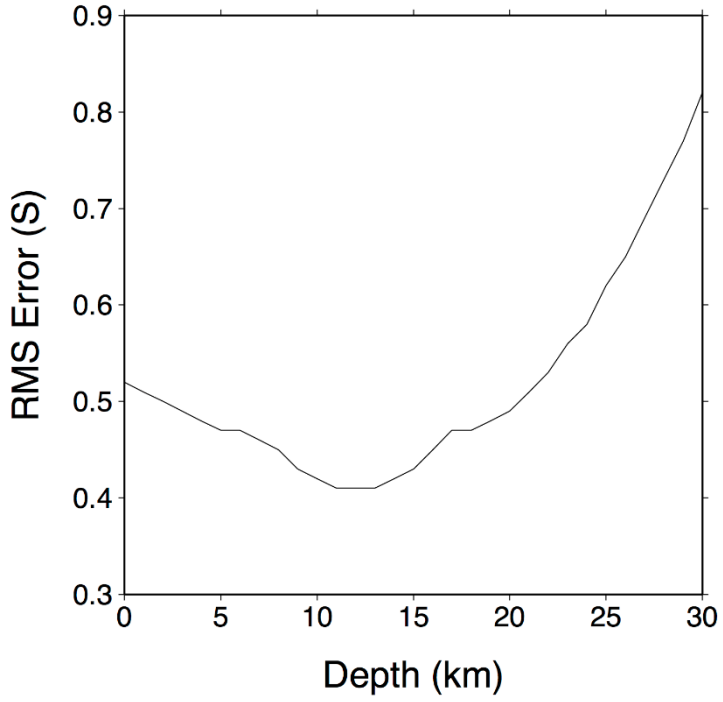

Figure 5. RMS error in earthquake location as a function of depth.

3 Magnitude

3.1 LOCAL MAGNITUDE

A local magnitude of 4.0 ± 0.2 ML was computed for the mainshock as the average of estimates derived from the largest S-wave amplitudes at 24 stations in the distance range 62 km to 588 km. The amplitudes were measured on horizontal component simulated Wood–Anderson records. Amplitudes were measured on both horizontal components giving 48 readings. The ML formula derived for California by Hutton and Boore (1987) is currently used for determination of earthquake magnitude in the UK.

$$ML = \log_{10} A + 1.11 \log_{10} r + 0.00189\, r - 2.09$$

where the amplitude A is in nanometres and the distance r is in kilometres.

A histogram determined from the individual magnitude readings is shown in Figure 6.

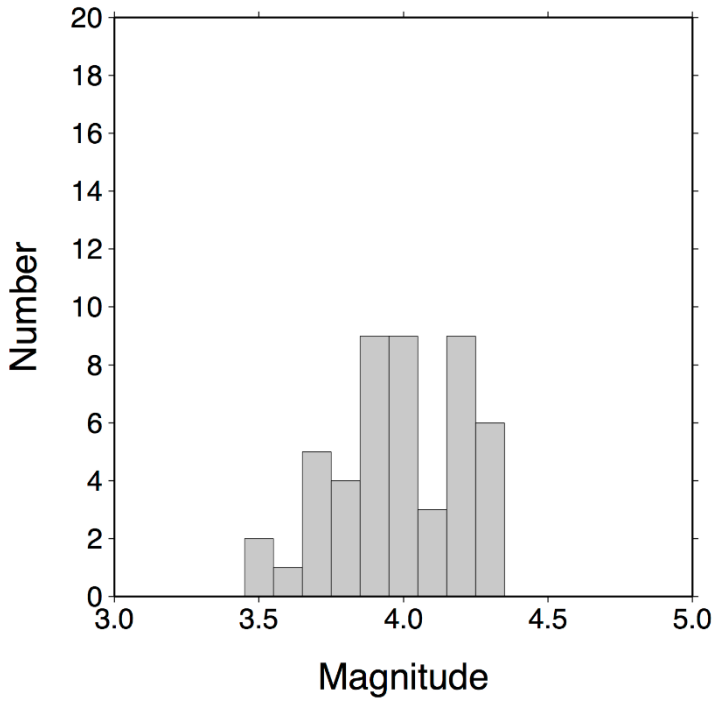

Figure 6. Histogram of individual magnitude readings.

3.2 MOMENT MAGNITUDE

We determined the seismic moment, M_0, and the stress drop, $\Delta\sigma$, of the mainshock by modelling the source displacement spectra. We use the spectral fitting method of Ottemöller and Havskov (2003), where M_0 and the corner frequency, f_c, are determined using a grid search. The observed spectra, $A(f)$, are corrected for instrument response and for the effects of geometrical spreading, G, and frequency dependent attenuation, $D(f)$. We also correct for the effect of the free surface, F, and the source radiation pattern, R, using correction factors of 2.0 and 0.6, respectively. The instrument response the observed displacement spectrum is given by

$$A(f) = G\ M_0\ R\ F\ S(f)\ D(f)$$

Following Herrmann and Kijko (1983), we assume geometrical spreading for *S*- and *Lg*-waves

$$G(r) = f(x) = \begin{cases} r^{-1}, & r < 100 \\ (100\,r)^{\frac{-1}{2}}, & r \geq 100 \end{cases}$$

where r (km) is the hypocentral distance.

The correction for attenuation $D(f)$ is commonly constructed in two parts. The first part accounts for attenuation along the path described by $Q(f)$ and the second accounts for near-surface attenuation κ (sec) near the receiver (Singh et al., 1982)

$$D(f) = \exp\left[\frac{-\pi T f}{Q(f)}\right] exp(-\pi\kappa f)$$

where T (sec) is the travel time. We used the United Kingdom average attenuation model derived for L_g waves of Sargeant and Ottemöller (2009)

$$Q(f) = 266\ f^{0.53}$$

This attenuation model was derived assuming the same geometrical spreading as used here. In this analysis we use only vertical component data, which means that correction for site amplification is not required. Following Ottemöller and Sargeant (2010) we use κ=0.02 sec.

The seismic moment is then given by

$$M_0 = \frac{4\,\pi\,\rho\,v^3\,A_0}{G(r)\,D(f)F\,R}$$

where we use the density ρ=2.7 g/cm^3 and the S-wave velocity at the source v_s = 3.5 km/sec, and A_0 is the amplitude of the flat part of the spectrum $A(f)$.

We use the ω^2 model (Aki, 1967; Brune, 1970) for the shape of the earthquake source spectrum $S(f)$, where

$$S(f) \propto \frac{1}{(f/f_c)^2 + 1}$$

The observed and modelled spectra are shown in Figure 7. In general the modelled spectra provide a good fit for the observations at all stations. Similarly, the observed spectra show good signal-to-noise levels at frequencies above the corner frequency. The average value for Mw determined from the 14 observations is 3.6 ± 0.1.

We compute the source radius r (km) from the corner frequency f_c (Brune, 1970)

$$r = 0.37\,v_s/f_c$$

The stress-drop $\Delta\sigma$ (bar) is given by

$$\Delta\sigma = 0.44M_0/r^3$$

assuming a circular fault (Eshelby, 1957). We find average values for the source radius and stress drop of 0.572 ± 0.277 km and 17.2 ± 14.5, respectively. The large uncertainty in the stress drop reflects the station-to-station variability of the corner frequency measurement.

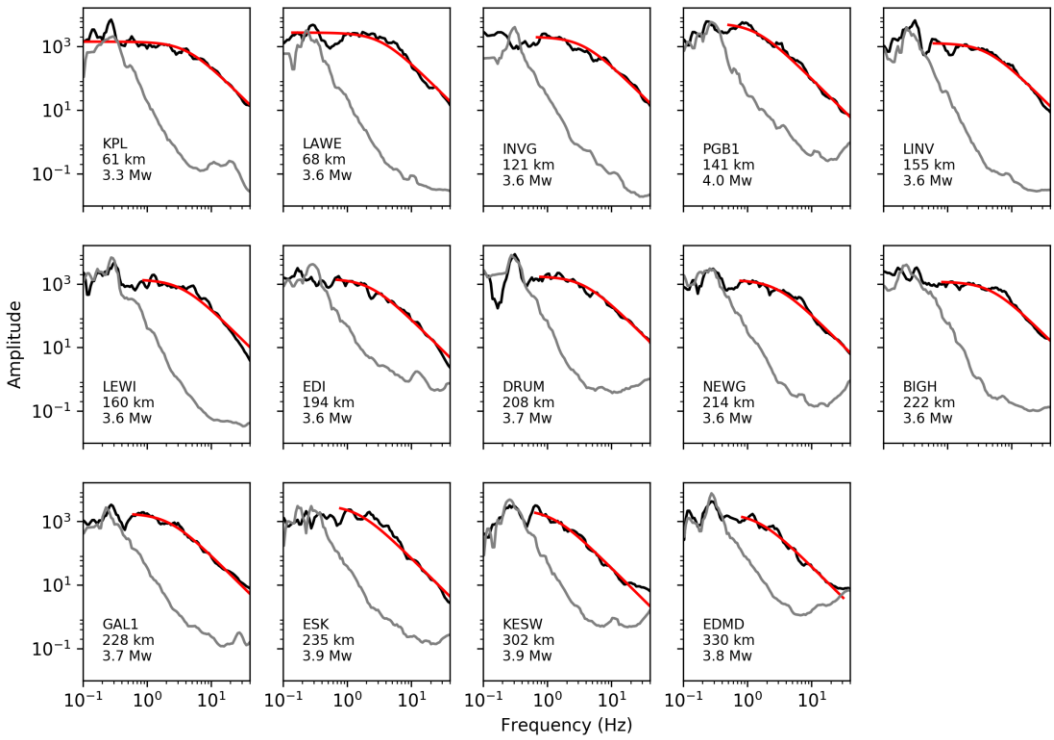

Figure 7. Observed displacement spectra (black) at the stations used to determine Mw. The red line shows the modelled displacement spectrum and the grey line shows the amplitude of the noise.

4 Focal Mechanism

Focal mechanisms for the earthquake were determined from measured first motion polarities on the vertical component of ground motion and SH/P amplitude ratios using three different methods: FOCMEC, the grid search method of Snoke et al. (1984); HASH (Hardebeck and Shearer, 2003); and, FPFIT, Reasenberg and Oppenheimer [1985]. Both FOCMEC and HASH use both polarities and SH/P amplitude ratios. FPFIT uses only polarities. The 1-D velocity model and the best fitting hypocentre were used to determine take-off angles.

We measured 11 first motion polarities and 5 SH/P amplitude ratios. The stations where these were measured are shown in Figure 8 (a) and (b). Sampling of the focal sphere is quite poor as a result of the large azimuthal gap with all the measurements from either the east of the epicentre.

For the grid search method of Snoke et al. (1984), we used a grid spacing of 2° and a maximum amplitude ratio error of 0.1. 21 solutions were found that fitted the data. These were all very similar and we selected the one with the smallest amplitude ratio error as representative. We also used a grid spacing of 2° for HASH along with a maximum average error in the amplitude ratio of 0.1.

The source mechanisms given by the three different methods are shown in Figure 8 (c), (d) and (e). All three methods show a right-lateral predominantly strike-slip fault that strikes north-northwest south-southeast and dips by varying amounts to the west. The second fault plane calculated by both FOCMEC and FPFIT strikes approximately east-west and dips north. However, HASH calculates a second fault plane that is near vertical and strikes northeast-southwest (d). These results suggest that the mechanism is not very well constrained.

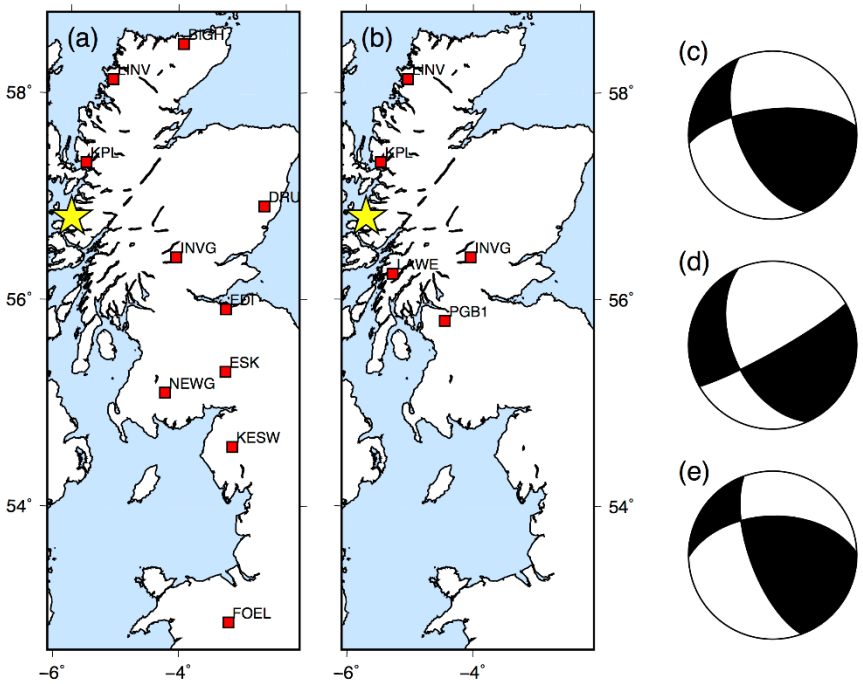

Figure 8. Stations where first motion polarities (a) and SH/P amplitude ratios were measured. Source mechanisms determined using (c) FOCMEC, (d) HASH and (e) FPFIT.

5 Aftershocks

The earthquake was followed by at least four aftershocks, the largest of which had a magnitude of 3.4 ML and which occurred two minutes after the mainshock. The two largest aftershocks were also felt by people across the region. Measured P- and S-wave arrival times were used to determine hypocentres for each of four aftershocks using the HYPOCENTER location algorithm (Lienert et al., 1986) in the same way as for the mainshock. Similarly, local magnitudes were also calculated using measured amplitudes. Source parameters for all five earthquakes are shown in Table 3. There is some scatter in the calculated hypocentres, but in general the epicentres are within a few kilometres. The depths are rather more scattered. Estimated horizontal and vertical errors for the smaller events are significantly larger than for the bigger ones, primarily as a result of fewer measured phases.

Date	Time (UTC)	Latitude	Longitude	Depth	ML	Npha	GAP	RMS	ERX	ERY	ERZ
04/08/2017	14:43:38.70	56.805	-5.888	12.2	4.0	33	153	0.41	7.0	1.7	4.9
04/08/2017	14:45:34.10	56.798	-5.869	10.6	3.4	14	178	0.28	6.7	1.7	4.7
04/08/2017	15:20:24.00	56.804	-5.871	8.8	1.1	7	181	0.31	14.4	2.4	13.6
04/08/2017	16:07:26.50	56.794	-5.893	8.2	1.2	6	221	0.23	16.3	1.8	8.5
04/08/2017	17:35:06.30	56.807	-5.874	10.1	2.2	14	178	0.35	8.3	1.8	5.9

Table 3. Source parameters for the mainshock and four aftershocks. Npha is the number of phases used for the location, GAP is the azimuthal gap, RMS is the RMS error in the earthquake location, and ERX, ERY and ERZ are the errors in the X, Y and Z directions in kilometres.

Hypocentres and the 95% confidence ellipsoids for all five earthquakes are shown in Figure 9. Again, the horizontal error is much larger in the EW direction for all five events as a result of the distribution of stations and the large azimuthal gap.

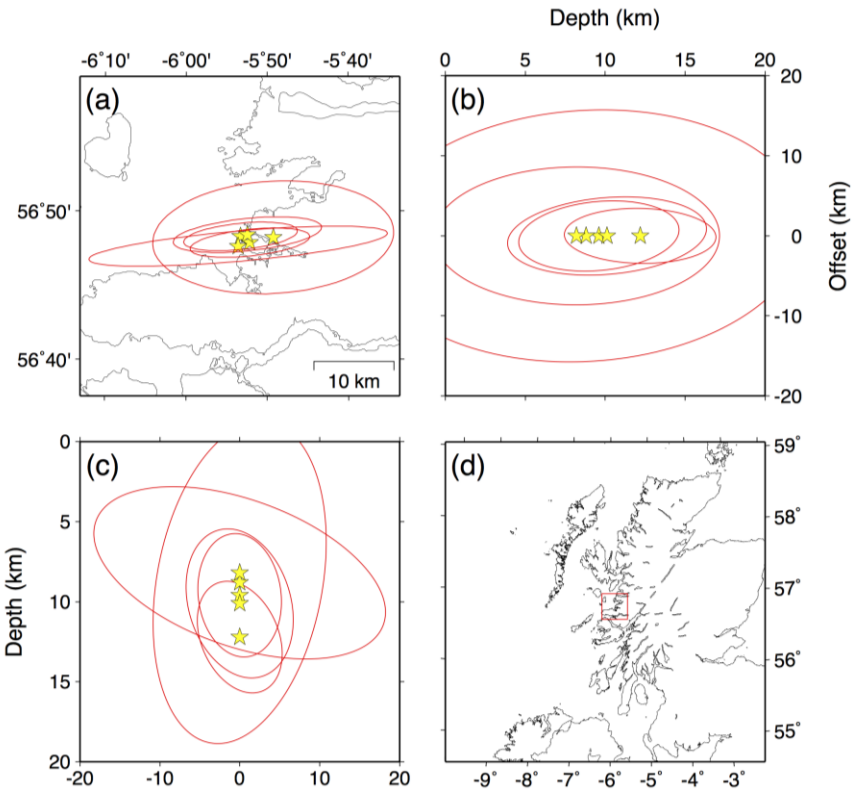

Figure 9. Projections of 95% confidence ellipsoid for each of the hypocentres in: (a) the horizontal (XY) plane; (b) the YZ plane; and (c) the XZ plane. Each plane shows an area of 20 km by 20 km. (d) Shows the location of (a).

To further compare the events, we examined waveforms from two of the closest stations KPL (61 km) and INVG (121 km). Figure 10 and Figure 11 show the ground motions recorded at KPL and INVG, respectively. Each trace shows one second before and three seconds after the P-wave arrival. All five traces on both stations are very similar, which suggests that all of the earthquakes are closely located and have similar fault mechanisms. For example, the first motion of the initial P-wave arrival at KPL is down on all traces and the first motion of the initial P-wave arrival at INVG is up. There are also similarities in the P-wave codas of each event, although some

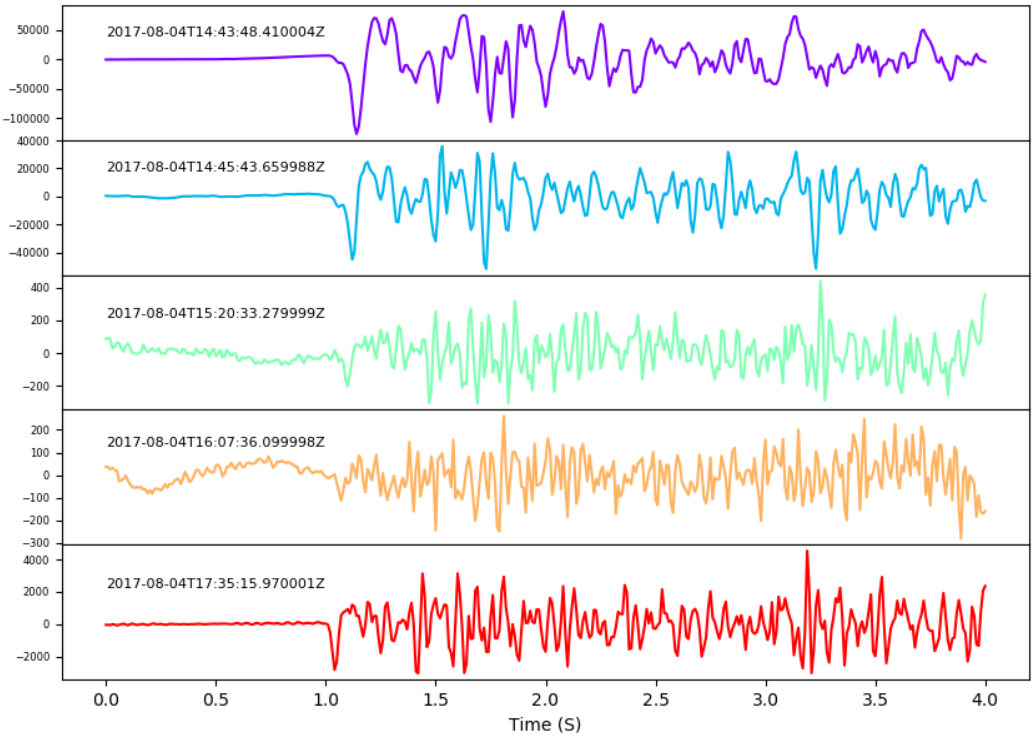

Figure 10. Ground motions (nm/s) for the five earthquakes recorded at KPL at a distance of 61 km from the epicentre. Each trace shows one second before and three seconds after the P-wave arrival.

differences are apparent. For example, the recording of the magnitude 1.2 ML event at 16:07 UTC at INVG has a high amplitude arrival approximately two seconds after the initial P-wave arrival that is not apparent on the other events. These differences may suggest some small variations in the event hypocentre and fault mechanism. In addition, the largest event shows a noticeably lower frequency content as might be expected for a higher magnitude.

Given the clustering of the hypocentres and the similarity of the observed waveforms, we used the double difference method (Waldhauser and Ellsworth, 2000) to determine relative locations for the five events in the sequence. The double difference method was used with both the measured phase-picks and precise relative travel-time differences obtained by cross-correlating the recorded waveforms at each station (e.g. Schaff and Richards, 2004). The double-difference residuals for pairs of earthquakes at each station were minimised by weighted least squares using singular value decomposition.

Figure 12 shows a comparison of the double difference locations with single event locations. The hypocentres are plotted in relation to the cluster centroid. The double differences locations are significantly more clustered than the single event locations, with some evidence for alignment of the hypocentres along an east-west trend at a depth of around 11 km. The relocated hypocentres all lie within a source with dimensions of 300m, 100m and 500m in the X, Y and Z directions respectively.

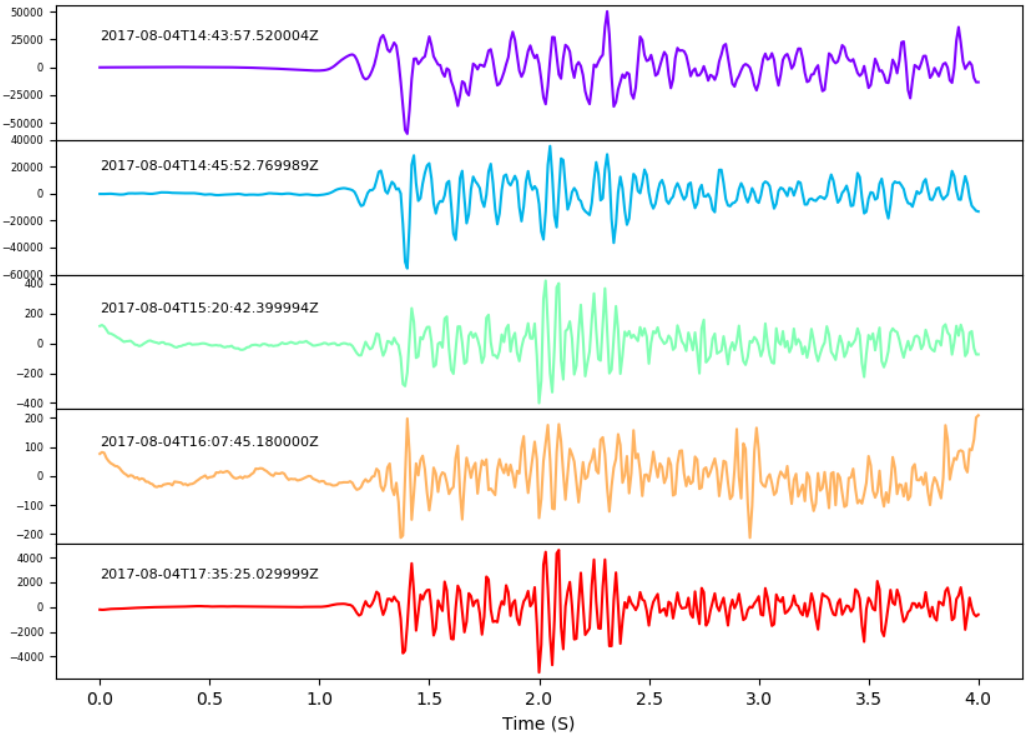

Figure 11. Ground motions (nm/s) for the five earthquakes recorded at INVG at a distance of 121 km from the epicentre. Each trace shows one second before and three seconds after the P-wave arrival.

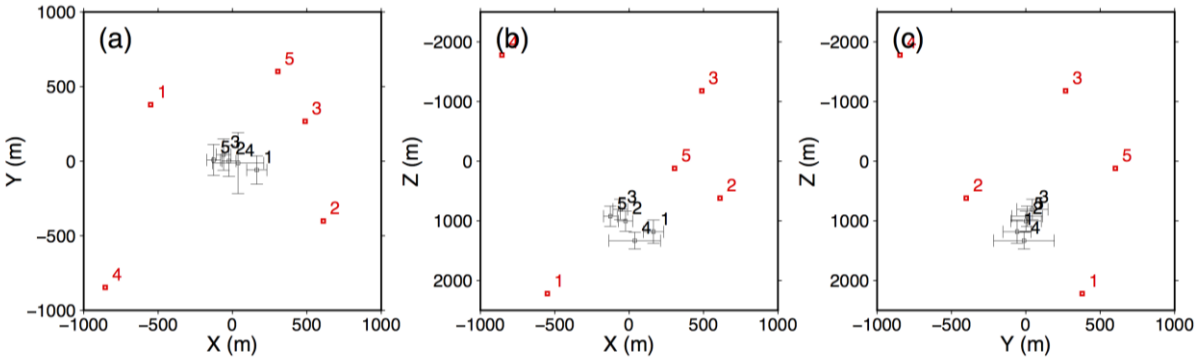

Figure 12. A comparison of the single event locations (red squares) with the locations from the double difference method (black squares with error bars) in the (a) XY, (b) XZ and (c) YZ planes. Hypocentres are plotted relative to the cluster centroid.

6 Macroseismic Observations

353 members of the public from 121 different postcodes completed our online macroseisemic questionnaire, allowing EMS intensity to be calculated in different locations. A minimum number of five reports from a given 5 km by 5 km square are required to estimate the intensity. Where

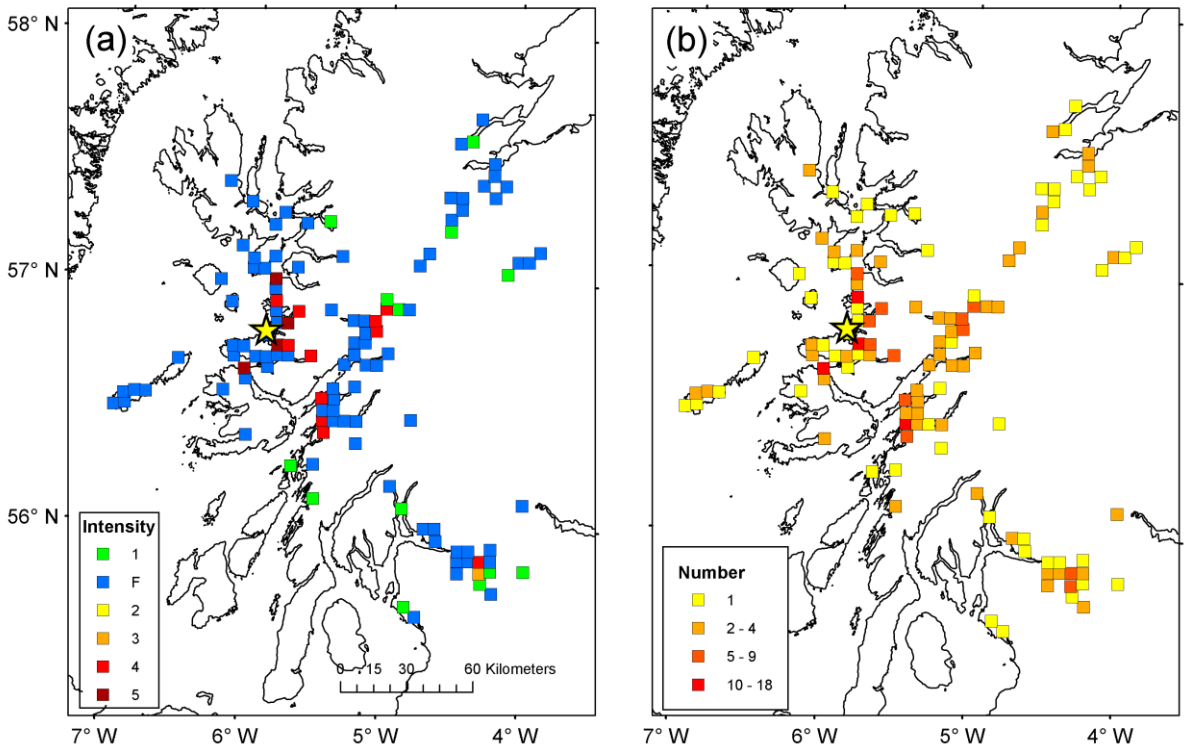

Figure 13. Coloured squares in (a) show intensities calculated from macroseismic data. (b) show the number of observations used to determine each intensity value.

there are fewer than 5 different observations, we assign an intensity value of "Felt". A maximum intensity of 5 EMS was observed in the villages of Acharacle and Roshven, 10 km from the epicentre. An intensity of 5 EMS was also observed at Tobermory and Mallaig, approximately 20 km from the epicentre. Intensities of 4 EMS were observed at Lochailort (10 km), Strontian (12 km) and Arisaig (12 km). There were too few observations to determine a value for the intensity from most of the other locations close to the epicentre, perhaps as a result of the low population density. Intensities of 4 EMS were observed in Oban and Fort William at distances of 45 km to the southeast and 48 km to the east, respectively. The earthquake was felt at distances of up to 150 km from the epicentre, including Inverness and Invergarry to the northeast and Glasgow to the southeast. Five reports from central Glasgow suggest an intensity of 4 EMS, however, this does not seem consistent with other observations.

Over half of the reports state that people considered the shaking to be moderate in strength, while around one third thought that it was weak. Many people reported hearing a moderate to loud bang or rumble. There were 31 reports of objects falling over but no reports of damage.

7 Discussion

Instrumental data have been used to determine a hypocentre and source mechanism for the Moidart earthquake. The distribution of stations means that the earthquake epicentre is well constrained in a north-south direction, but less so in an east-west direction. Focal depth is also less well constrained, though the distribution of RMS errors with depth shows a clear minimum at 12 km, suggesting that the earthquake most likely nucleated in the mid-Crust. Figure 14 (a) shows histograms of earthquake depths for earthquakes with magnitudes of 2.5 ML for both Scotland and all the British Isles. Earthquakes in both Scotland and the wider region have focal depths that are distributed though the upper part of the Crust. There is weak evidence for the hypothesis that larger earthquakes nucleate at greater depths (Figure 14 b).

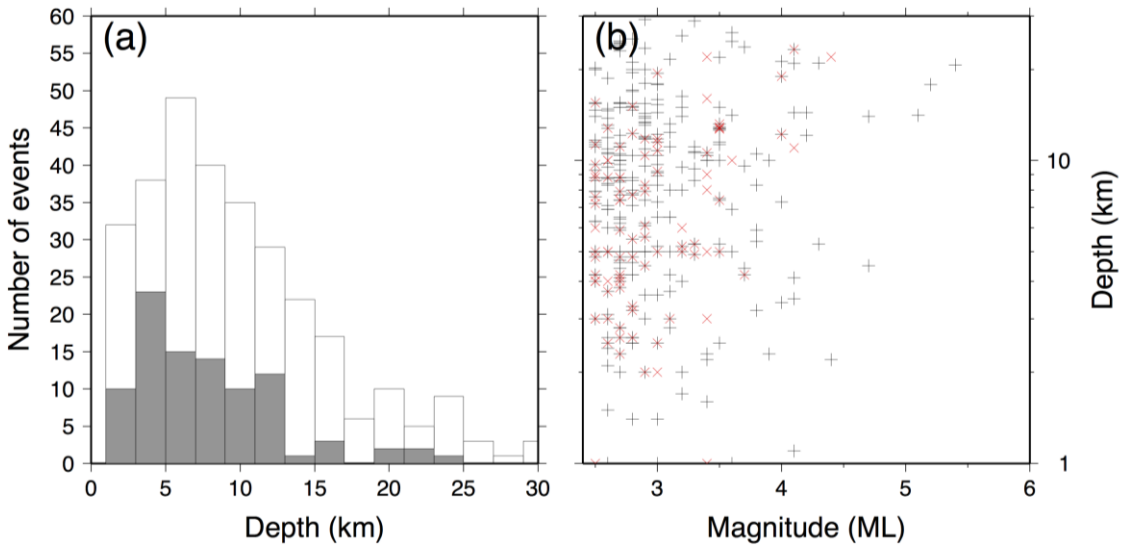

Figure 14. (a) Histogram showing the depth distribution for earthquakes with magnitudes of 2.5 ML or above in the BGS earthquake catalogue. Grey bars show earthquakes in Scotland only, white bars show all earthquakes in the British Isles and immediate offshore area. (b) Magnitude (ML) as a function of hypocentral depth. Grey crosses show all earthquakes. Red crosses show those in Scotland only.

In general, it is difficult to associate earthquakes in the British Isles with specific faults because: (a) no British earthquake recorded either historically or instrumentally has produced a surface rupture; (b) uncertainties in the earthquake location, especially depth, which are typically several kilometres; (c) uncertainties in fault distributions and orientation at depth; and, (d) the limited size of the earthquakes means the rupture dimensions are small. This is also the case for 2017 Moidart earthquake which has a calculated rupture area of approximately 1 km^2.

Figure 15 shows recorded earthquake activity in northwest Scotland along with major mapped faults from the British Geological Survey DigMapGB series. The faults are interpreted from field mapping, borehole information and seismic data and as such may not capture the full structural complexity of an area. Although the distribution of seismicity is rather diffuse, we suggest that most clusters of earthquake activity are associated with steeply dipping faults that strike

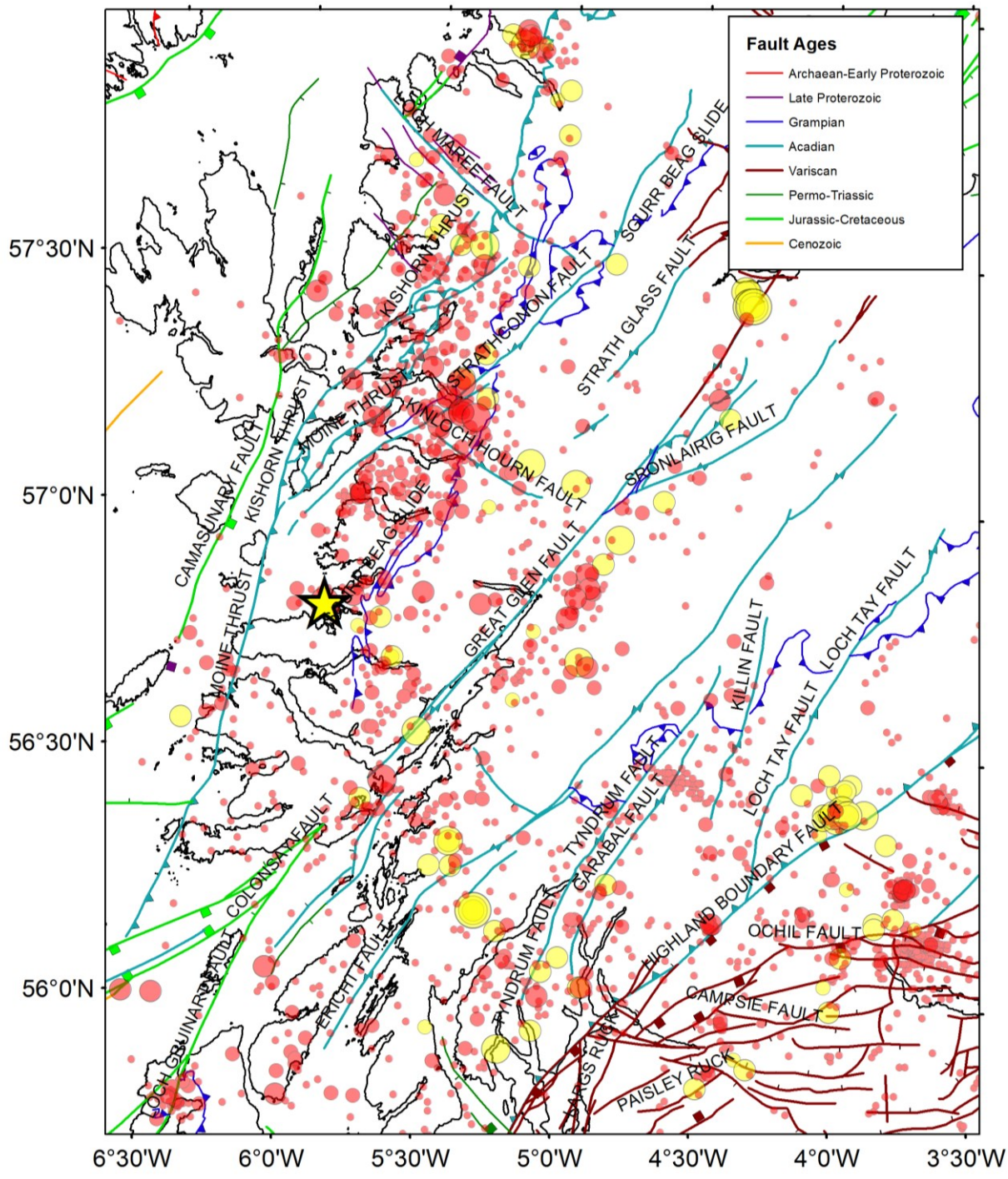

Figure 15. Instrumentally recorded earthquakes (red circles), from 1970 to present, and historical earthquakes (yellow circles), from 1700 to 1969, in northwest Scotland. Circles are scaled by magnitude. The epicentre of the Moidart earthquake of 4 August 2017 is indicated by the yellow star. Lines show mapped faults from the British Geological Survey DigMapGB series, ©NERC 2016. The faults are coloured by geological age.

approximately southwest-northeast or northwest-southeast and are thought to extend throughout the Crust. For example, the Great Glen fault, the Strathconon fault and Kinloch Hourn fault. Assumpçao (1981) suggests that the proximity of the hypocentre calculated for the 1974 Kintail earthquake to the Strathconon Fault, along with the agreement between the NE-SW strike of the fault and one of the calculated fault planes provides evidence that the earthquake took place on this fault. Similarly, events such as the Oban earthquake of 1986 and the Inverness earthquakes in 1816, 1890 and 1901 could be associated with reactivation of the Great Glen fault. By contrast,

low angle thrusts such as the Moine Thrust, the Kishorn Thrust and the Sgurr Beag Slide have significantly less earthquake activity associated with them. However, earthquake activity in the far northwest of Scotland appears to be bounded to the southeast by the Sgurr Beag Slide. No major faults have been mapped in the vicinity of the Moidart earthquake. However, it seems likely that this earthquake also occurred on a steeply dipping fault that strikes southwest-northeast or northwest-southeast.

Earthquake focal mechanisms provide both fault geometries and principal stress directions that can be used to constrain our understanding of the driving forces of current deformation. In areas of low seismicity and sparse station distribution, determining reliable focal mechanisms can be problematic. This means that available mechanisms for earthquakes in Scotland are limited to larger events of ML ≥ 3.5/4.0, as it is generally not possible to calculate mechanisms for smaller events (Baptie, 2010). Figure 16 shows focal mechanisms available for earthquakes in Scotland. Focal mechanisms for the Kintail, Carlisle and Aberfoyle earthquakes were published by

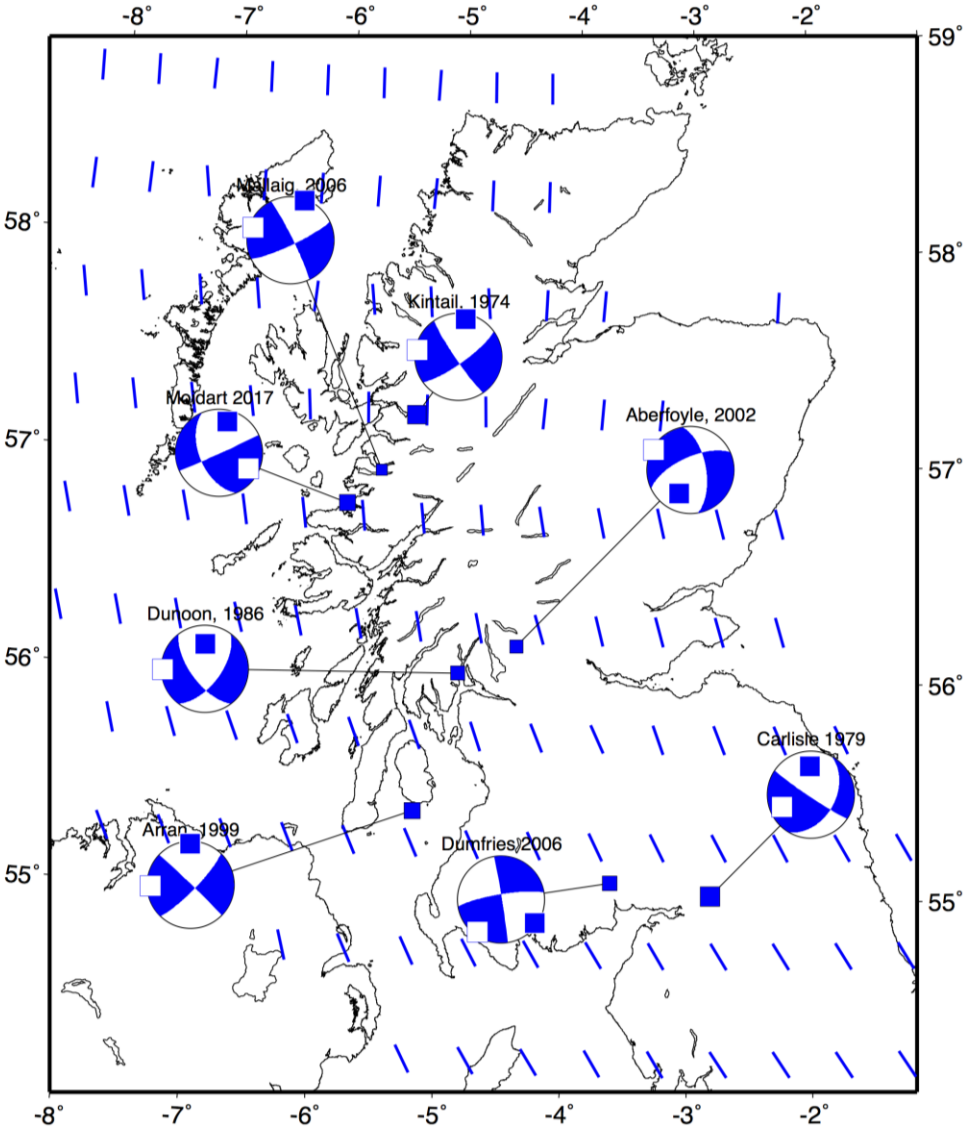

Figure 16. Focal mechanisms available for earthquakes in Scotland (Baptie, 2010). The blue and white areas show the compressional and dilatational quadrants and the lines between the quadrants show the strike and dip of the two possible fault planes. The axes of maximum and minimum compression are indicated by the blue and white squares respectively. The blue squares on the map show the location of the earthquakes. The blue lines show the orientation of the maximum horizontal compressive stress, sH, taken from smoothed stress orientations published in the World Stress Map (Heidbach et al., 2010).

Assumpçao (1981), King (1980) and Ottemöller and Thomas (2007). The mechanisms for the Dunoon, Arran, Dumfries and Mallaig earthquakes were published by Baptie (2010). The mechanism shown for the Moidart earthquake is the one determined using the program HASH.

All the focal mechanisms consistently show strike-slip faulting with N-S compression and E-W tension. This results in either left-lateral strike-slip faulting along near vertical NE-SW fault planes, or right-lateral strike-slip faulting along near vertical NW-SE fault planes. The fault planes are generally steeply dipping, though there is some variation in both the angle and direction of dip (e.g. Dunoon, 1985; Aberfoyle, 2002). Although the mechanism determined for the Moidart earthquake is probably poorly constrained, it does show good agreement with the previously published mechanisms.

The World Stress Map (Heidbach et al., 2010) contains sH (maximum horizontal compressive stress) orientations for the British Isles determined from a variety of stress indicators including borehole breakouts (e.g. Williams et al., 2015), drilling induced fracturing and hydro-fracturing as well as previously published focal mechanisms. Figure 15 also shows smoothed stress orientations on a 0.5° grid from the World Stress Map. The orientation of sH is roughly N-S in the north of Scotland, rotating to a more NW-SE direction in the north of England. This agrees reasonably with the focal mechanisms in Scotland. However, the smoothed sH values are based on sparse data, with most borehole breakout data from offshore areas (e.g. Williams et al., 2015).

Left-lateral strike-slip along a NE-SW trend is consistent with the prevailing N- to NNW-oriented horizontal tectonic stresses of western Europe (Grunthal and Stromeyer, 1992), and the earlier Palaeocene and Oligocene Alpine-related compression. This trend matches the recent geological history of the large-scale fault structures in British Isles where Alpine-related compression has driven faulting. This means that faults such as the Great Glen fault or Strathconon fault, which strike NE-SW are likely to show left-lateral strike-slip. Similarly, steeply dipping faults that strike NW-SE will have right lateral strike-slip.

This suggests that earthquake activity in northwest Scotland is a result of re-activation of a number of favourably oriented, steeply dipping fault systems, by deformation associated with first order plate motions rather than deformation associated with glacio-isostatic recovery (e.g. Muir-Wood, 2000).

8 Conclusions

The 2017 Moidart earthquake occurred in the mid-Crust at a depth of approximately 12 km. This is largely consistent with observed focal depths for other earthquakes in the region, which are distributed throughout the upper 20 km of the Crust.

The calculated focal mechanism suggests that the earthquake resulted from strike-slip faulting on a fault plane that strikes either SW-NE or NW-SE and dips steeply, although the dip of both fault planes is rather poorly constrained. This is in good agreement with focal mechanisms calculated for other earthquakes across the region, which all show similar solutions.

Seismicity in northwest Scotland is clustered around a number of large, steeply dipping major faults that strike either NE-SW or NW-SE suggesting that earthquake activity across the region is driven by reactivation of such fault systems by deformation associated with first order plate motions rather than deformation associated with glacioisostatic recovery.

Although there are no mapped major fault systems in the immediate vicinity of the Moidart earthquake, the similarity of the focal mechanism to others calculated in the region suggests that it also resulted from slip on an unmapped fault that strikes NE-SW or NW-SE.

The mainshock and the aftershocks all occurred within a small source volume, of the order of a few hundred metres in extent and had similar source mechanisms.

The modelled source displacement spectra provide a good fit for the observed displacement spectra and suggests a moment magnitude of 3.6 ± 0.1. This is slightly less than that expected for an earthquake with a local magnitude of 4.0 ML using the well-known empirical relationship determined by Grunthal et al (2009), which gives an expected moment magnitude of 3.7 Mw. This discrepancy has implications for seismic hazard estimation and requires further research.

References

AKI, K., 1967. Scaling law of seismic spectrum. *J. Geophys. Res.*, 72, 1217–1231.

ASSUMPCÃO, M., 1981. THE NW SCOTLAND EARTHQUAKE SWARM OF 1974. *Geophys. J. Roy. Astr. Soc.* 67, 577–586.

ASSUMPCÃO, M. AND BAMFORD, D., 1978. LISPB V. Studies of crustal shear waves. *Geophys. J. R. Astron. Soc.* 54, 61–73.

BAMFORD, D., NUNN, K., PRODEHL, C., JACOB, B., 1978. LISPB-IV. Crustal structure of Northern Britain. *Geophys. J. R. Astron. Soc.* 54, 43– 60.

BAPTIE, B. 2010. Seismogenesis and state of stress in the UK. Tectonophysics 482 (2010) 150–159

BRUNE, J. N., 1970. Tectonic stress and the spectra of seismic shear waves from earthquakes. *J. Geophys. Res.*, 75, 4997–5009.

ESHELBY, J., 1957. The determination of the elastic field of an ellipsoidal inclusion and related problems. *Proc. R. Soc. London A* 241, 376–396.

EVERNDEN, J.F., 1969. Precision of epicenters obtained by small numbers of world-wide stations. *Bulletin of the Seismological Society of America*, 59, 1365–1398.

GRUNTHAL, G., STROMEYER, D., 1992. The recent crustal stress field in central Europe: trajectories and finite element modeling. J Geophys Res.

GRUNTHAL, G., WAHLSTRÖM, R. AND STROMEYER, D. 2009. The unified catalogue of earthquakes in central, northern, and northwestern Europe (CENEC)—updated and expanded to the last millennium. *Journal of Seismology*, 13, 517–541

HARDEBECK, J. L. AND SHEARER, P. M., 2003. Using S/P Amplitude Ratios to Constrain the Focal Mechanisms of Small Earthquakes. *Bulletin of the Seismological Society of America*, 93:2434-2444.

HERRMANN, R. B., AND A. KIJKO, A, 1983. Modeling some empirical vertical component Lg relations. *Bulletin of the Seismological Society of America* 73, 157–171.

HUTTON, L. K., AND D. M. BOORE, 1987. The ML scale in southern California. *Bulletin of the Seismological Society of America,* 77, 2074–2094.

KING, G., 1980. A fault plane solution for the Carlisle earthquake, 26 December 1979. Nature 286, 142–143.

LIENERT, B. R. E., BERG, E., AND FRAZER, L. N., 1986. HYPOCENTER: An earthquake location method using centered, scaled, and adaptively least squares. *Bulletin of the Seismological Society of America*, 76:771-783.

MUIR-WOOD, R., 2000. Deglaciation Seismotectonics: a principal influence on intraplate seismogenesis at high latitudes. *Quaternary Science Reviews*, 19, 1399-1411

MUSSON, R M W. 1994. A catalogue of British earthquakes. *British Geological Survey Global Seismology Report*, WL/94/04.

Musson, R. M. W. 1996. Determination of parameters for historical British earthquakes. *Annali di Geofisica*, 39, 1041-1048.

OTTEMÖLLER, L., AND J. HAVSKOV, 2003. Moment magnitude determination for local and regional earthquakes based on source spectra. *Bulletin of the Seismological Society of America*, 93, 203–214.

OTTEMÖLLER, L., THOMAS, C.W., 2007. Highland Boundary Fault Zone: Tectonic implications of the Aberfoyle earthquake sequence of 2003. *Tectonophysics*, 430, 83–95.

OTTEMÖLLER, L. AND SARGEANT, S. 2010. Ground-Motion Difference between Two Moderate-Size Intraplate Earthquakes in the United Kingdom. *Bulletin of the Seismological Society of America*, 100, 4, 1823–1829

SARGEANT, S., AND L. OTTEMÖLLER, 2009. Lg wave attenuation in Britain. *Geophys. J. Int.* 179, no. 3, 1593–1606.

REASENBERG, P. AND OPPENHEIMER, D., 1985. FPFIT, FPPLOT, and FPPAGE: Fortran computer programs for calculating and displaying earthquake fault plane solutions. Technical report, U.S. Geol. Survey.

SCHAFF, D. P., AND RICHARDS, P.G. 2004. Repeating seismic events in China. *Science*, 303, 1176–1178.

SINGH, S. K., R. J. APSEL, J. FRIED, AND J. N. BRUNE, 1982. Spectral attenuation of *SH* waves along the Imperial fault. *Bulletin of the Seismological Society of America*, 72, 2003–2016.

SNOKE, J., MUNSEY, J., TEAGUE, A., BOLLINGER, G., 1984. A program for focal mechanism determination by combined use of polarity and P-SV amplitude ratio data. *Earthquake Notes* 55, 3–15.

WALDHAUSER, F. AND ELLSWORTH, W.L., 2000. A double-difference earthquake location algorithm: method and application to the Northern Hayward Fault, California. *Bulletin of the Seismological Society of America,* 90, 1353–1368.

WILLIAMS, J. D. O., FELLGETT, M. W., KINGDON A., AND WILLIAMSON, J. P. 2015. In-situ stress orientations in the UK Southern North Sea: Regional trends, deviations and detachment of the post-Zechstein stress field. Marine and Petroleum Geology, 67, 769-784.